Cement and Concrete Research 40 (2010) 1350–1359

Contents lists available at ScienceDirect

Cement and Concrete Research

journal homepage: http://ees.elsevier.com/CEMCON/default.asp

Composition, morphology and nanostructure of C–S–H in 70% white Portland cement–30% fly ash blends hydrated at 55 °C.

A.V. Girão [a], I.G. Richardson [a,*], R. Taylor [a], R.M.D. Brydson [b]

[a] School of Civil Engineering, University of Leeds, Leeds LS2 9JT, United Kingdom
[b] Institute for Materials Research, University of Leeds, Leeds LS2 9JT, United Kingdom

ARTICLE INFO

Article history:
Received 10 October 2008
Accepted 17 March 2010

Keywords:
Fly ash (D)
C–S–H (B)
Temperature (A)
TEM (B)
NMR

ABSTRACT

Outer product C–S–H had a mixture of fibrillar and foil-like morphology in a 28-day-old water-activated paste, and foil- or lath-like morphology in an alkali-activated paste. It was not possible to determine the chemical composition of C–S–H using SEM-EDX because of fine-scale intermixing with other phases; TEM-EDX was necessary. The C–S–H formed in the alkali-activated paste had a lower mean Ca/(Al + Si) ratio than that formed with water. The mean length of the aluminosilicate anions in the C–S–H was similar in both systems and increased with age; those in the Op C–S–H were likely to be shorter than those present in the Ip C–S–H with water activation, but longer (and more protonated) with alkali. The potassium in the alkali-activated paste was present either within the C–S–H structure charge balancing the substitution of Al^{3+} for Si^{4+}, or adsorbed on the C–S–H charge balancing sulfate ions.

1. Introduction

The main binding phase in all Portland cement (PC)-based systems is a nearly amorphous or poorly crystalline calcium silicate hydrate (C–S–H). The physical properties of a hardened cement paste are as a consequence influenced strongly by the morphology and composition of the C–S–H, which are affected by many factors such as the composition of the cement, the water or solution/solid ratio, curing temperature, degree of hydration and the presence of chemical admixtures and supplementary cementing materials (SCM), such as ground granulated blast-furnace slag, metakaolin, or fly ash [1]. The temperature of curing has a significant impact on the development of the physical properties of a cement paste because it affects the kinetics of hydration and the distribution and nature of the hydration products [e.g. 2–11]. Understanding the effects of high temperatures on cement hydration (i.e. <100 °C at atmospheric pressure) is relevant in a number of situations in practice, including hot weather climates, accumulated heat evolution, and heat curing to accelerate strength gain (e.g. in precast products). The aim of this work was to determine the effect of curing at 55 °C on the composition, morphology and nanostructure of C–S–H formed in blends of PC with 30% fly ash, activated with either distilled water or 5 M KOH solution; results for neat PC hydrated at 55 °C and both neat PC and PC-30% fly ash blends hydrated at 85 °C have been published recently in references [12] and [13] respectively. As in the work reported in those articles, KOH solution was used here to activate one of the pastes because the resulting C–S–H is structurally better ordered than that formed with water activation. This increased order results in narrower linewidths in solid-state ^{29}Si magic angle spinning nuclear magnetic resonance (MAS NMR) spectra; individual peaks are consequently much better resolved, which makes deconvolution of the spectra relatively straightforward. The results of the deconvolution of the NMR spectra for the KOH-activated pastes are then used to facilitate the deconvolution of the spectra for those activated with water, as in previous work on blends involving blast-furnace slag [14,15] and metakaolin [16]. Pastes were examined at 1 day and 28 days using solid-state ^{29}Si MAS NMR, backscattered electron imaging with energy dispersive X-ray analysis (EDX), thermal analysis with evolved gas analysis, and X-ray diffraction (XRD); the 28-day-old samples were also examined by transmission electron microscopy (TEM) with EDX analysis.

2. Experimental

Pastes with 70% white Portland cement (WPC; Castle Cement Limited, Clitheroe, U.K.) and 30% class F fly ash (PFA 8109, Drax, Selby, U.K.) were hand mixed to a water or solution to solid ratio of 0.5 (ml/g), with distilled water or with a 5 M KOH solution. The oxide compositions for the anhydrous WPC and fly ash obtained by X-ray fluorescence spectroscopy (XRF) are given in Table 1. The samples were cast in 7 ml polystyrene tubes, sealed in polyethylene bags and cured in a water bath at 55 ± 1 °C.

XRD measurements were performed using a Panalytical X'Pert-Pro diffractometer system (with X'Celerator real time multiple strip detector), operated with Cu Kα radiation at 40 mA and 45 kV. The samples were demoulded, sliced using a slow-speed cut-off saw and mounted on a sample holder that was spun at 2 rps. XRD acquisition was carried out in continuous scan mode over the range 6.03 to 54.95°

* Corresponding author.
E-mail address: I.G.Richardson@leeds.ac.uk (I.G. Richardson).

0008-8846/$ – see front matter © 2010 Elsevier Ltd. All rights reserved.
doi:10.1016/j.cemconres.2010.03.012

Table 1
Bulk oxide composition for the WPC and PFA determined by XRF.

Oxide (wt.%)	WPC	PFA
SiO_2	24.81	52.92
Al_2O_3	2.35	26.85
Fe_2O_3	0.49	8.64
MgO	0.80	1.65
CaO	68.61	4.49
Na_2O	0.15	1.20
SO_3	2.03	0.44
K_2O	0.06	3.26

2θ with a step width of 0.01675° (i.e. 2921 steps) and a counting time of 34.29 s, corresponding to a total acquisition time of nearly 14 min.

The quantity of calcium hydroxide in the pastes was determined by thermogravimetric analysis (STA1500, Stanton Redcroft, London, U.K.). Samples were freshly crushed and ground to a powder in an agate mortar, and were heated to 1000 °C at 20 °C/min, under a constant flow of nitrogen. An evolved gas analysis (EGA) system (Cirrus mass spectrometer, MKS Spectra Products Ltd., U.K.) interfaced with the STA equipment was used to differentiate mass loss associated with water or carbon dioxide: CO_2 was not detected in any of the samples thus confirming that no carbonation occurred during sample preparation.

Solid-state ^{29}Si single-pulse MAS NMR spectra were acquired using a Varian InfinityPlus 300 spectrometer (magnetic field 7.05 T; operating frequency of 59.5 MHz for ^{29}Si). Paste samples were freshly ground after 1 day and 28 days hydration. Samples were packed into 6 mm zirconia rotors sealed at either end with Teflon end plugs, and spun at 6 kHz in a Chemagnetics-style probe. The spectra were acquired over 10,000 scans using a pulse recycle delay of 2 or 5 s, a pulse width 2 or 4 μs, and an acquisition time 20 ms. Quantitative information on the fractions of Si present in silicate tetrahedra with different connectivities was obtained by deconvolution of the single-pulse spectra. The fitting procedure involved the subtraction of a contribution from a spectrum taken from anhydrous cement, which thus accounted for the unreacted alite and some of the belite, followed by the iterative fitting of peaks for belite, fly ash and C–S–H using IgorPro 5.0 (Wavemetrics, Inc., U.S.A.). The spectra were initially fitted using three peaks for the C–S–H (Q^1, Q^2(1Al) and Q^2(0Al) at approximately −79, −81.5 and −85 ppm respectively) but this was found to be unsatisfactory because the Al/Si ratio calculated using the deconvoluted peak intensities was higher than that measured directly by TEM-EDX, which is in contrast with results for a number of other systems (for example see Fig. 17 in [15]) but is consistent with recent work by Taylor et al. [17] on mature slag-Portland cement blends (the mean aluminosilicate chain length and the mean Al/Si ratio of the C–S–H were calculated from the integrated peak intensities using Eqs. (1) and (2) in [18]). The same spectrum-fitting issues as discussed by Taylor et al. were encountered in this work, and the same approach adopted, which essentially involved the inclusion of a fourth C–S–H peak by the simple allocation of a proportion of the Q^2(1Al) peak to one not associated with Al (Q^{2B}, see discussion in [17]) such that the Al/Si ratio calculated from the integrated peak intensities was the same as that measured by TEM-EDX. Whilst a peak for fly ash was removed during deconvolution, it was found that it was impossible to quantify the extent of reaction because for the fly ash (but not the other peaks), the ratio of the signal in the centre band to that in the sidebands varied unpredictably with age; further work is required to determine the reasons for this. As a consequence, quantitative information on the degree of reaction is not given.

For scanning electron microscopy with energy dispersive X-ray analysis (SEM-EDX), the samples were demoulded and cut into 400 μm thick slices, using a slow-speed cut-off saw with a diamond wafering blade. The samples were dried by solvent exchange with propan-2-ol. The slices were then impregnated with epoxy-resin (Epofix Kit, Struers) under vacuum and, after hardening, polished to a flat surface on a rotary grinding/polishing machine (PdM-Force20 mounted on Struers Rotopol-35), using silicon carbide paper of different grades (600–2400 grit from Struers, Glasgow, UK). The samples were subsequently polished with diamond paste (3, 1 and 0.25 μm). The surface of the polished samples was carbon coated in a vacuum coating unit (EMSCOPE TB500, U.K.) and analyzed in an SEM (CamScan Series 4, U.K., equipped with an UTW EDX detector, Oxford, U.K., and ISIS software for imaging/X-ray analysis, Oxford Instruments) at an accelerating voltage of 20 kV and working distance of 28 mm. The images in this article were obtained using a Philips XL-30 SEM operated at 20 kV and at working distances between 7.7 and 8.1 mm.

Transmission electron microscopy with energy dispersive X-ray analysis (TEM-EDX) was used to examine the morphology of the C–S–H and to determine its chemical composition (Philips CM20, Eindhoven, Netherlands, equipped with an UTW EDX detector, Oxford, U.K., and ISIS software for imaging/X-ray analysis, Oxford Instruments). For TEM, 200 μm-thick slices were hand thinned, using silicon carbide paper of different grades (600–2400 grit from Struers, Glasgow, UK), until they were approximately 30 μm thick. Ni grids with a 2×1 mm slot were glued onto both sides of the sample as a 'sandwich'. The specimens were then argon ion-beam milled (Model 1010 Ion Mill, Fischione Instruments, PA, U.S.A.) using a liquid nitrogen cooled stage in order to avoid excessive specimen heating and consequent damage. The specimens were carbon coated after milling. Around 50 EDX analyses were taken of regions in each of the 28-day-old samples. Each region was checked before EDX analysis by selected area electron diffraction (SAED) for the presence of crystalline phases. This strategy ensured that analyses were obtained of C–S–H free of intermixture with other phases, except AFt, which is sufficiently unstable in the microscope that it loses structural order and consequently gives no crystalline reflections (i.e. spots) on the electron diffraction pattern; mixtures of C–S–H with AFt were therefore identified on the basis of morphology and compositional trends and such analyses were excluded when calculating mean compositions for C–S–H.

3. Results and discussion

3.1. X-ray diffraction and thermal analysis

XRD showed that the crystalline phases present in the 1-day-old water-activated paste included some residual alite and belite, CH and AFt. By 28 days, more of the cement had reacted and the main crystalline hydration products were CH, AFt and AFm, which was not detected by XRD in the equivalent neat cement paste [12]. The 28-day-old KOH-activated paste had some unreacted cement but no AFm or AFt; the peaks for CH were broad, indicating a small average crystal size, as observed previously in the neat cement paste [12] and in other KOH-activated systems [e.g. 16]. Mullite was present in both pastes (from the fly ash) and the KOH-activated paste contained a small amount of hydrogarnet (but much less than in the equivalent paste hydrated at 85 °C [13]).

The quantity of CH in the pastes determined by thermogravimetry is given in Table 2 (as a percentage of ignited weight). At both 1 and

Table 2
Results from thermal analysis and the deconvolution of the single-pulse ^{29}Si NMR spectra for water- and KOH-activated samples hydrated for 1 and 28 days. MCL = mean aluminosilicate chain length for C–S–H. B = bridging tetrahedra occupied by Al / bridging tetrahedra occupied by Al and Si. %CH = calcium hydroxide as % of ignited weight determined by thermogravimetry.

	% CH	Al/Si	MCL	B (%)	B_w/B_{KOH} (%)
1 d water	13	0.08	4.1	46	73
1 d KOH	13	0.12	4.0	63	
28 d water	12	0.16	15.6	48	74
28 d KOH	11	0.21	10.4	65	

28 days, KOH activation resulted in essentially the same amount of CH present as with water activation, which is in contrast with the neat cement pastes, where KOH activation resulted in a greater amount [12]. EGA showed unequivocally that the pastes had not carbonated, in agreement with the absence from the XRD traces of peaks for any of the polymorphs of calcium carbonate.

3.2. ^{29}Si NMR of pastes hydrated for 1 day and 28 days

Fig. 1 shows the single-pulse ^{29}Si NMR spectra for both the water- and KOH-activated pastes after 1 and 28 days hydration. As in previous studies [12–15] activation with KOH led to better-resolved peaks for C–S–H indicating a greater degree of structural order. The results of the deconvolution of the spectra for C–S–H are given in Table 2. The mean length of the aluminosilicate anions (represented by the mean chain length, MCL, in Table 2) in the C–S–H after hydration for 1 day was 4 for both water and KOH activation, which is slightly higher than in the neat cement paste (3.5) [12]. After 28 days the MCL had increased considerably in both cases: to about 16 with water and 10 with KOH, indicating that the aluminosilicate chains were either mainly heptakaidecameric or hendecameric with water or KOH respectively, or mixtures of dimers with very long chains. The proportion of occupied bridging sites in the dreierkette chains occupied by Al^{3+} and not Si^{4+} remained essentially unchanged between 1 and 28 days with both water and KOH activation (46–48% and 63–65% with water and KOH respectively). As a consequence the ratio of B_w/B_{KOH} is about ¾ at both ages; in other words, KOH activation produces around 1.3 times as much aluminium substitution as does water. Interestingly, this value is the same as that observed previously for ground granulated blast-furnace slag/WPC blends with 50 and 90% slag [14]. Whilst it was not possible to quantify the extent of cement and fly ash reactions (for the reason given in Section 2), nevertheless, comparison of the quantity of CH and the Al/Si ratio of C–S–H with the values for the neat cement pastes [12], indicates that some fly ash had reacted at 1 day, and a considerable amount by 28 days.

3.3. Backscattered electron imaging with X-ray analysis

The microstructure of the water-activated sample was quite porous after one day of hydration, with areas of CH, fly ash and partially reacted cement particles (that were often surrounded by Ip C–S–H), and many small fully reacted particles. An illustrative backscattered electron (BSE) micrograph of an area in the 1-day-old paste is shown in Fig. 2, which includes some labelled examples of calcium hydroxide (CH), fly ash (PFA), unreacted cement (U) and inner product C–S–H (Ip). Whilst some of the fully reacted particles appeared to be hollow, most contained some product, which is shown

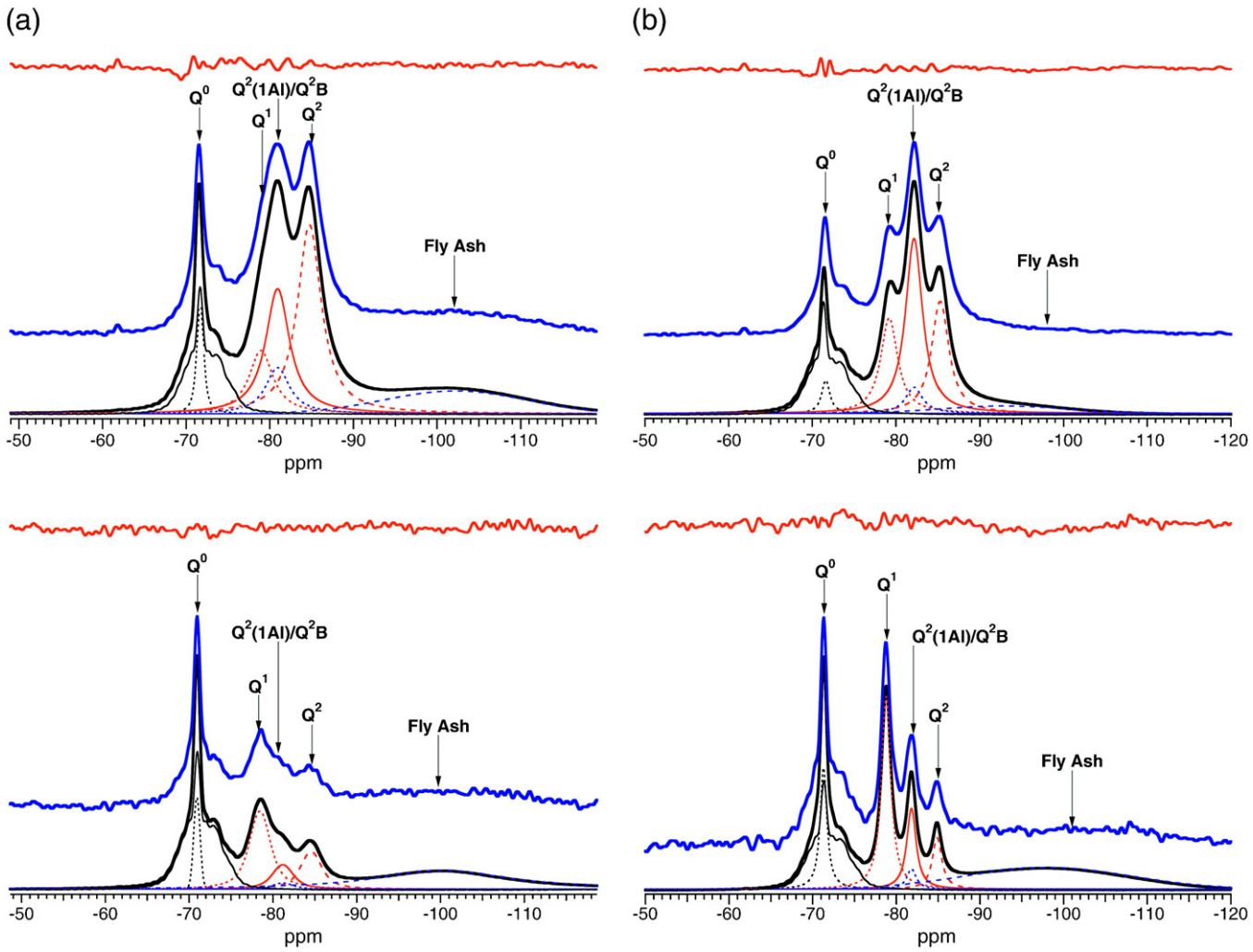

Fig. 1. Single-pulse ^{29}Si MAS NMR spectra for water-activated (a) and KOH-activated (b) pastes hydrated for 1 (bottom) and 28 days (top). All spectra are scaled to their tallest peak. The chemical shifts of the hydrate peaks (in ppm) in the order Q^1, $Q^2(1Al)/Q^{2B}$, $Q^2(0Al)$ are: −78.8, −81.8, −84.9 for 1 day-KOH; −78.9, −81.9, −85.0 for 28 day-KOH; −78.6, −80.6, −84.4 for 1 day-water; −78.9, −80.9, −84.7 for 28 day-water. The figures include the experimental spectrum (middle), the fitted peaks (bottom), and the residual (top; ×1). The larger of the two superposed peaks at around −81/−82 ppm is $Q^2(1Al)$ and the other is Q^{2B}.

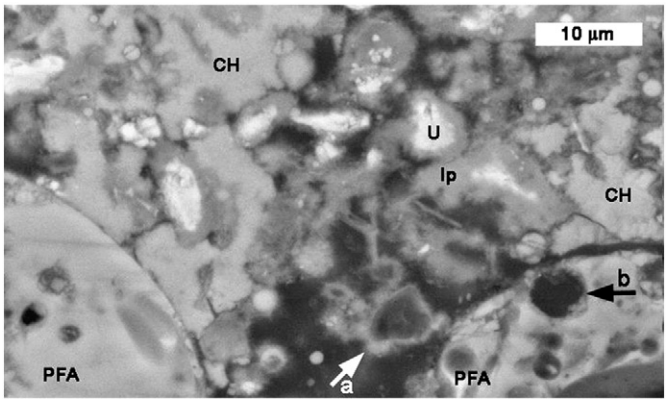

Fig. 2. Backscattered electron micrograph of an area in the 1-day-old water-activated blend. Regions of calcium hydroxide (CH), fly ash (PFA), unreacted cement (U) and dense inner product C–S–H are labelled. There are a number of small fully hydrated particles with dense rims, the largest of which is indicated with a white arrow (a); comparison with the resin-filled pore indicated by a black arrow (b) shows that the particle clearly contains material, which is presumably low-density inner product C–S–H.

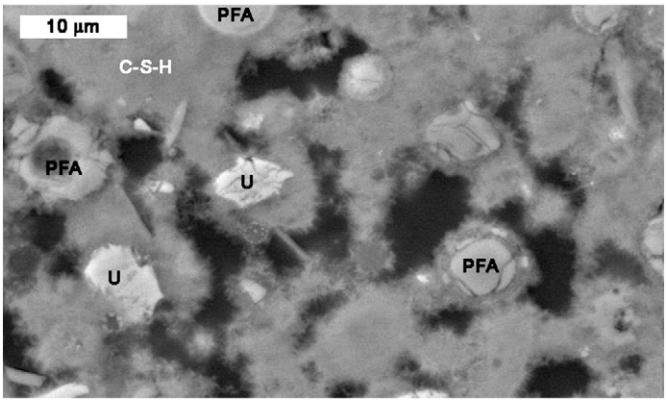

Fig. 4. A backscattered electron micrograph that illustrates an area of porous microstructure (part of Fig. 3 at higher magnification). Regions of unreacted fly ash (PFA), unreacted cement (U) and C–S–H are labelled; fibrils of outer product C–S–H can be seen protruding into the large pores.

in Section 3.4 by TEM to be a low-density Ip C–S–H (as observed previously in many other systems (see for example [15]): a number of small fully hydrated particles with dense rims are present on Fig. 2, the largest of which is indicated with a white arrow (labelled 'a'); comparison with the resin-filled pore indicated by a black arrow ('b') shows that the particle contains material.

After hydration for 28 days, the water-activated sample generally had a much denser microstructure due to the formation of more outer product (Op) C–S–H because of the greater extent of cement and fly ash hydration, although there were still extensive regions of high porosity. Fig. 3 is a low-magnification BSE micrograph that shows examples of both dense and porous microstructure; a large region of calcium hydroxide (CH) is labelled. Two regions in the micrograph — indicated by darker shaded rectangular areas — are shown at higher magnification in Figs. 4 and 5. Fig. 4 shows an area of porous microstructure; regions of unreacted fly ash (PFA), unreacted cement (U) and C–S–H are labelled, and fibrils of outer product C–S–H can be seen protruding into the large pores. Fig. 5 shows an area of dense microstructure; the black arrows indicate an almost fully reacted particle that has a dense rim of C–S–H with less-dense inner product. Fig. 6 is another low-magnification BSE micrograph that has examples of both dense and porous microstructure. The darker shaded rectangular area is again shown at higher magnification (in Fig. 7); this example of porous microstructure also contains plates of AFm, which is consistent with the XRD data.

An attempt was made to determine the chemical composition of C–S–H in the samples by EDX analysis in the SEM; points were selected for statistical analysis on the basis of compositional trends

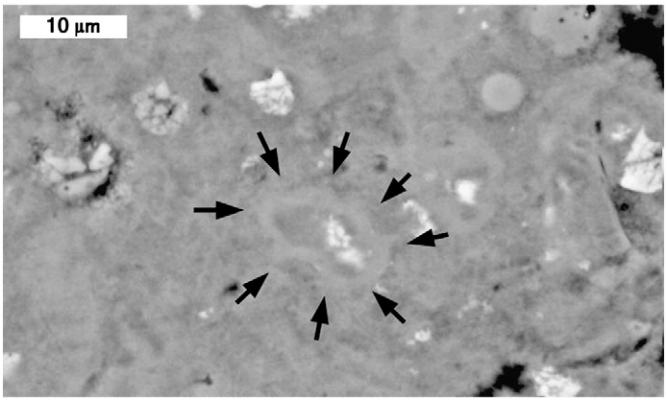

Fig. 5. A backscattered electron micrograph that illustrates an area of dense microstructure (part of Fig. 3 at higher magnification). The black arrows indicate an almost fully reacted particle that has a dense rim of C–S–H with less-dense inner product.

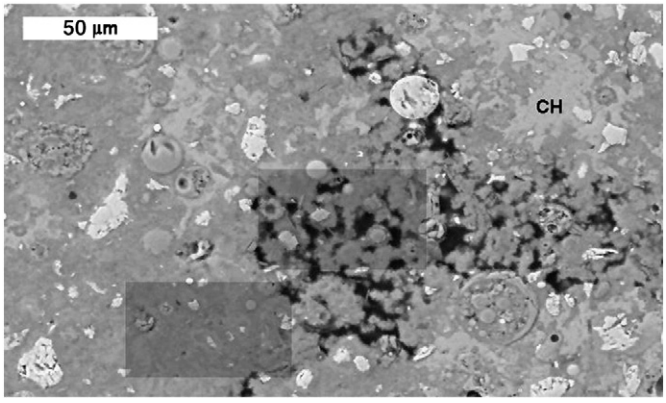

Fig. 3. A low-magnification backscattered electron micrograph of an area in the 28-day-old water-activated blend. A large region of calcium hydroxide (CH) is labelled. The area was selected because it contains examples of both dense and porous microstructure, both of which occurred extensively in the sample. The darker shaded rectangular areas are shown at higher magnification in Figs. 4 (porous microstructure) and 5 (dense microstructure).

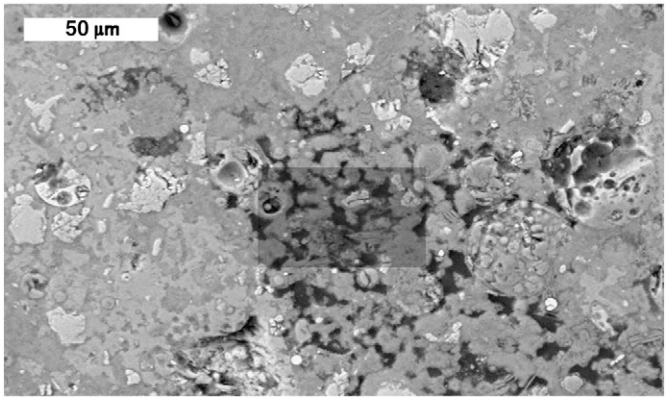

Fig. 6. A low-magnification backscattered electron micrograph of an area in the 28-day-old water-activated blend, again containing examples of both dense and porous microstructure, both of which occurred extensively in the sample. The darker shaded rectangular area is shown at higher magnification in Fig. 7 (porous microstructure).

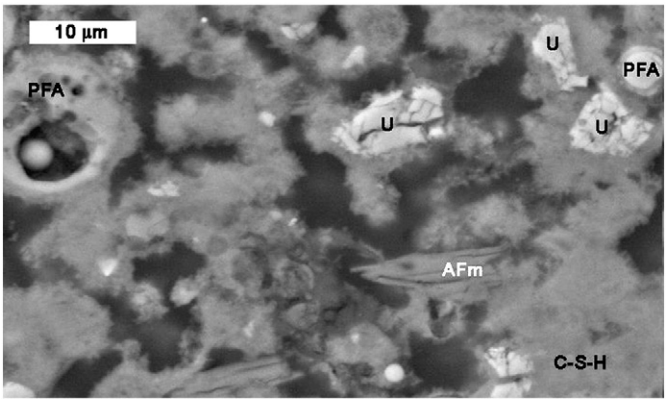

Fig. 7. A backscattered electron micrograph that illustrates an area of porous microstructure (part of Fig. 6 at higher magnification). Regions of unreacted fly ash (PFA), unreacted cement (U), C–S–H, and plates of AFm are labelled; fibrils of outer product C–S–H can be seen protruding into the large pores.

and microstructural location. The data for the 28-day-old samples with both water and KOH activation are plotted as Al/Ca against Si/Ca atom ratio scatter diagrams in Fig. 8; mean Ca/Si and Al/Si ratios for both 1 and 28 days are given in Table 3. For both methods of activation, the Ca/Si ratios at 28 days are statistically significantly lower than those at 1 day, and the Al/Si ratios are significantly higher; both of which are consistent with a greater level of fly ash reaction at 28 days. Interestingly, the data for the KOH-activated paste (Fig. 8 (bottom)) are distributed along a straight line towards the origin, which suggests that many of the analyses are due to various levels of intermixture between C–S–H and CH. The SEM-EDX data are compared in Section 3.4 with the compositions determined by TEM-EDX of C–S–H unambiguously free of intermixing with other phases.

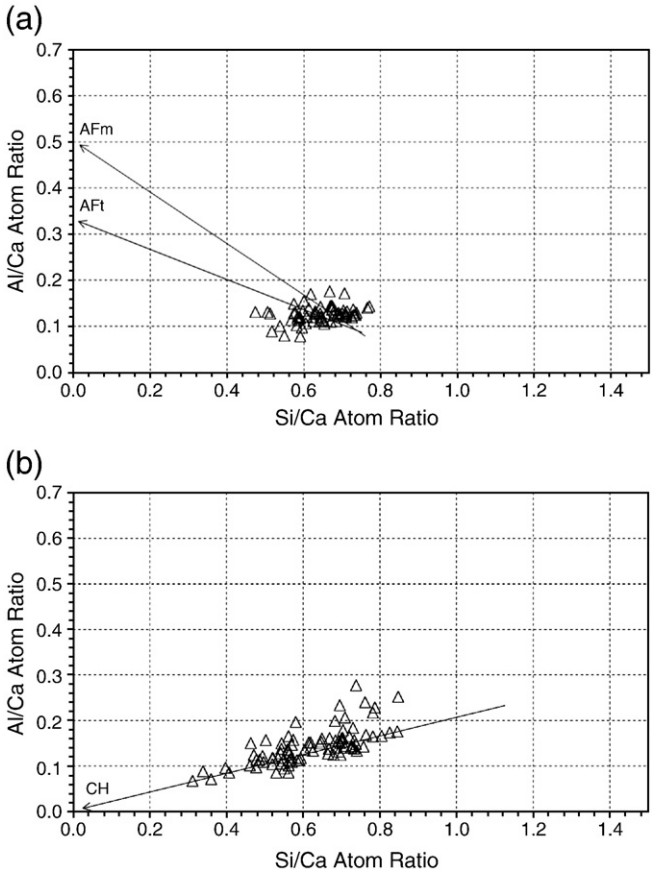

Fig. 8. Al/Ca against Si/Ca atom ratio plots of SEM-EDX analyses of 'C–S–H' present in the water-activated (a) and KOH-activated (b) pastes hydrated for 28 days.

Table 3
Mean Ca/Si and Al/Si atom ratios obtained for 'C–S–H' using SEM-EDX (S.D. = standard deviation; N = number of analyses) in both water- and KOH-activated pastes hydrated for 1 and 28 days.

	1 day				1 month			
	water	S.D. $N=86$	KOH	S.D. $N=84$	water	S.D. $N=69$	KOH	S.D. $N=87$
Ca/Si	1.83	0.39	1.92	0.63	1.57	0.17	1.68	0.38
Al/Si	0.15	0.09	0.19	0.04	0.20	0.03	0.23	0.04

3.4. Transmission electron microscopy with X-ray analysis

Samples of both the water- and KOH-activated pastes that had been hydrated for 28 days were examined by TEM. The Op C–S–H in the water-activated paste was often essentially fibrillar and very fine, which is illustrated in Fig. 9; this micrograph also includes relicts of AFt intermixed with the C–S–H. As well as fibrillar Op C–S–H, the sample also contained Op C–S–H that had a crumpled-foil morphology, which is illustrated in Fig. 10; foil-like morphology is typical of Op C–S–H that has low Ca/(Si + Al) ratio (see [19] and references therein).

As noted in Section 3.3, BSE images of the water-activated paste show many fully reacted particles with dense rims that appear to contain a lower density inner product. This conclusion is confirmed by TEM: two examples of fully, or almost fully, reacted particles are shown in Figs. 11 and 12. The Ip C–S–H is foil-like in both cases — although coarser in Fig 12 than in Fig. 11 — and surrounded by dense rims and fibrillar Op C–S–H. A third example is shown in Fig. 13, which contains mainly coarse foil-like C–S–H, although it is somewhat finer at the centre of the particle. Although not confirmed by X-ray analysis (because analyses were not undertaken) the thin laths on the micrograph are probably a hydrotalcite-like phase — as observed by TEM in fly ash blends at lower temperature [20] — and the dark features are most likely unreacted glassy fly ash; there are also some small relicts of AFt. Interestingly, the Ip C–S–H present in partially reacted fly ash particles often had a more linear, fibrillar morphology, albeit not as fine featured as the surrounding Op C–S–H; good examples are shown in Fig. 14 for the water-activated paste (which is similar to Fig. 3 in [20]) and Fig. 15 for the KOH-activated paste.

The morphology of Op C–S–H that is formed with KOH activation is foil- and lath-like rather than fibrillar. Good illustrative examples of

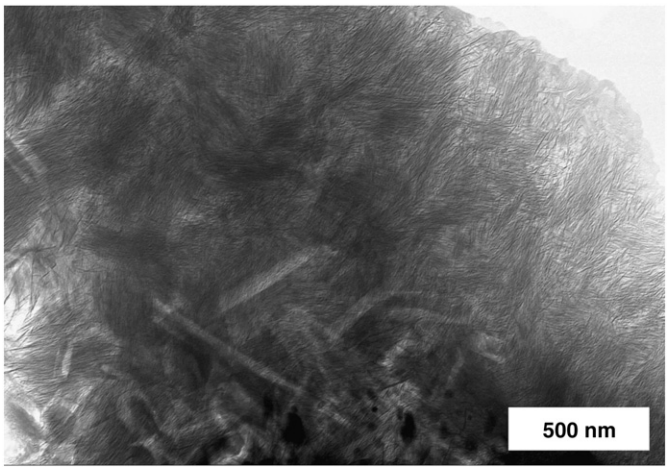

Fig. 9. A TEM micrograph from the water-activated paste hydrated for 28 days showing fine fibrillar Op C–S–H and relicts of AFt.

Fig. 10. A TEM micrograph from the water-activated paste hydrated for 28 days showing both fibrillar and foil-like Op C–S–H.

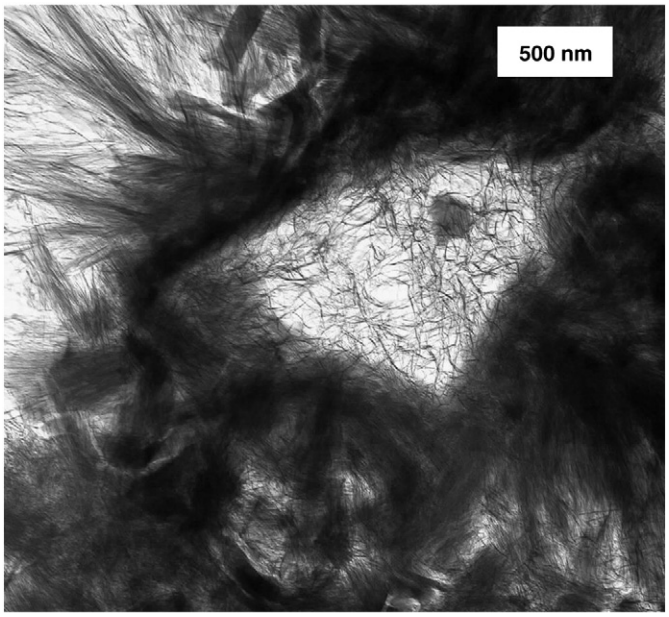

Fig. 12. A TEM micrograph from the water-activated paste hydrated for 28 days showing fibrillar Op C–S–H (with some relicts of AFt) surrounding a small fully reacted particle containing low-density foil-like Ip C–S–H.

both morphologies are shown in Fig. 16 (bottom and right-hand side). The laths appear to consist of stacks of very poorly ordered layers, which merge with the crumpled foils. The microcrystalline nature of CH in the KOH-activated paste indicated by XRD was confirmed by TEM; an example is shown in Fig. 16 (left, top and middle) where the

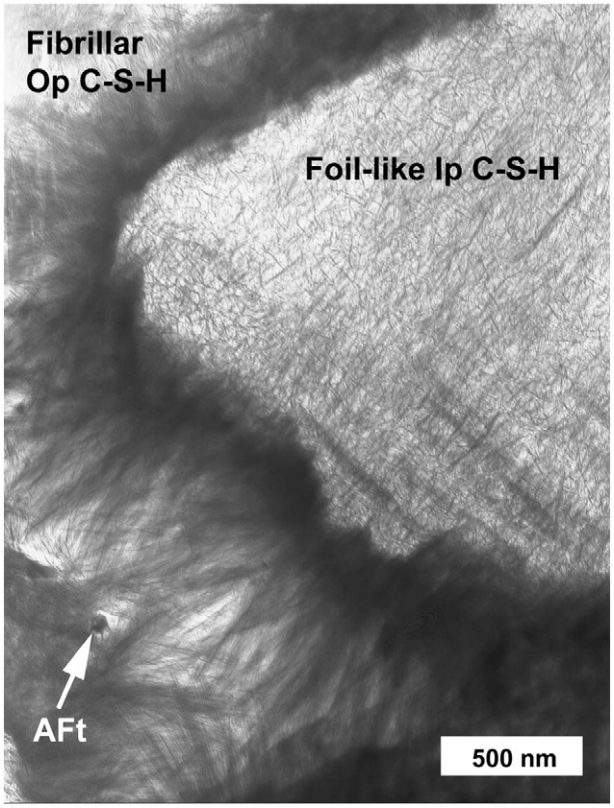

Fig. 11. A TEM micrograph from the water-activated paste hydrated for 28 days showing fine fibrillar Op C–S–H (with a small relict of AFt) surrounding low-density foil-like Ip C–S–H.

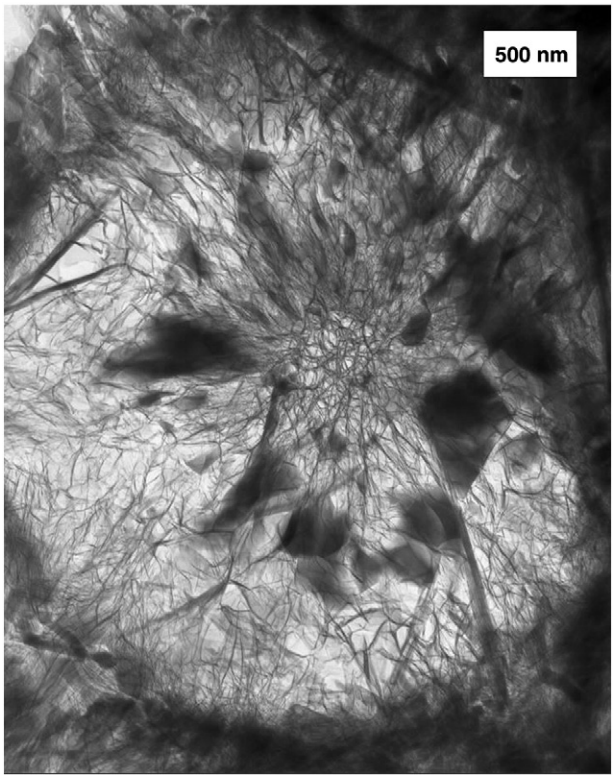

Fig. 13. A TEM micrograph from the water-activated paste hydrated for 28 days showing an almost completely hydrated PFA particle; the Ip C–S–H has foil-like morphology.

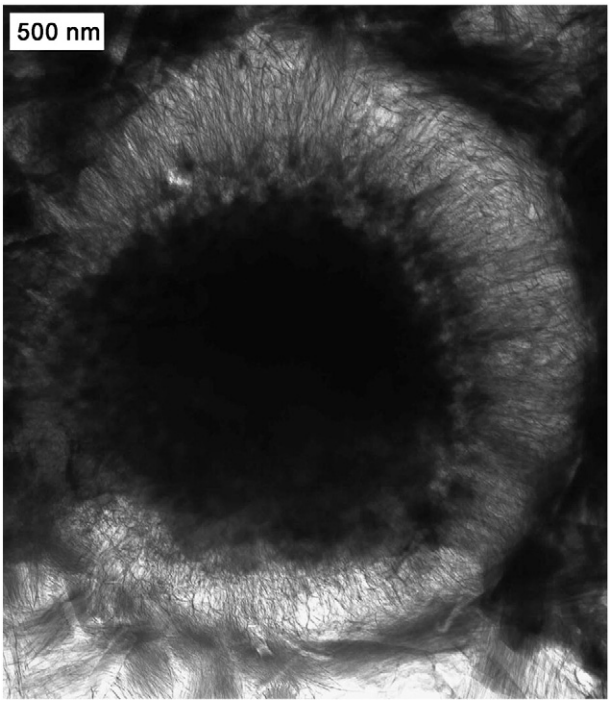

Fig. 14. A TEM micrograph from the water-activated paste hydrated for 28 days showing a partially hydrated PFA particle.

CH microcrystals appear dark where they are oriented such that they diffract electrons strongly; the microcrystals of CH in these regions are interstratified with layers of C–S–H.

EDX analyses were taken from areas of Ip and Op C–S–H approximately 200 nm in diameter, in both the water and KOH-activated pastes. Analyses for the water-activated paste are plotted in Figs. 17 and 18, and analyses for the KOH-activated paste are plotted in Figs. 19–21. It was sometimes difficult in the water-activated paste to select areas totally free of thin laths of AFm or relicts of AFt, which, because they are partially decomposed, cannot be discarded on the basis of the presence of crystalline reflections on a SAED pattern. The difficulty can perhaps be appreciated by examining the Op region in Fig. 9 where fibrillar Op C–S–H is intermixed with relicts of AFt; for example, the linear striations in the bottom half and left-hand-side of the micrograph are AFt relicts. Analyses of such mixtures will of course contain enhanced amounts of Ca, Al and S and were excluded when calculating mean compositions for the C–S–H. Four analyses in the water-activated paste were taken of AFm crystals, which are represented by filled triangles on Figs. 17 and 18; it is clear that the

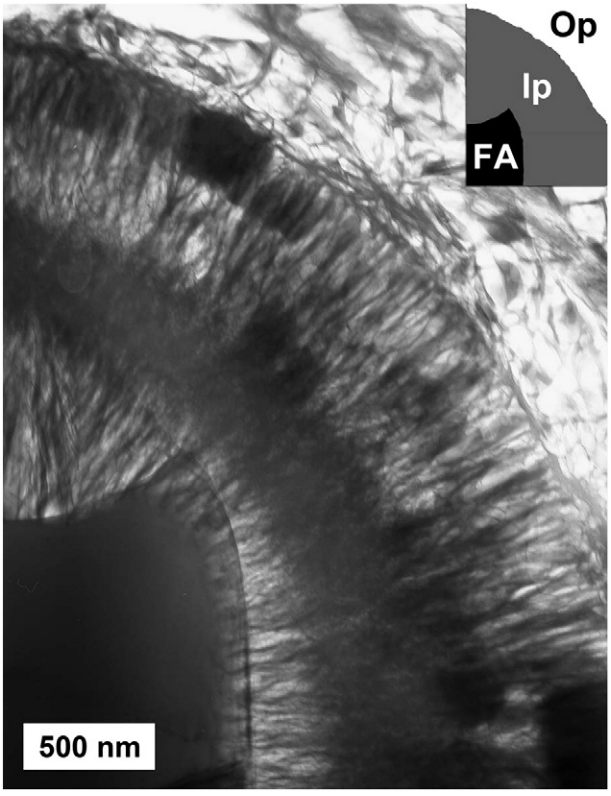

Fig. 15. A TEM micrograph from the KOH-activated paste hydrated for 28 days showing a partially hydrated PFA particle.

Fig. 16. A TEM micrograph from the KOH-activated paste hydrated for 28 days showing microcrystalline CH intermixed with C–S–H (left) and foil-like Op C–S–H (right and bottom).

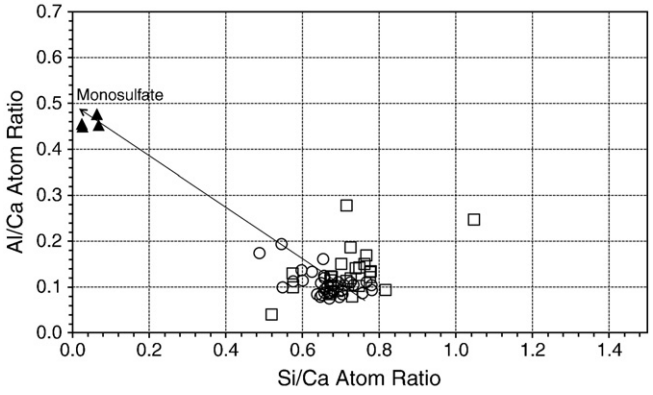

Fig. 17. Al/Ca against Si/Ca atom ratio plot of TEM-EDX analyses of AFm (▲) and Op (○) and Ip (□) C–S–H present in the water-activated paste hydrated for 28 days.

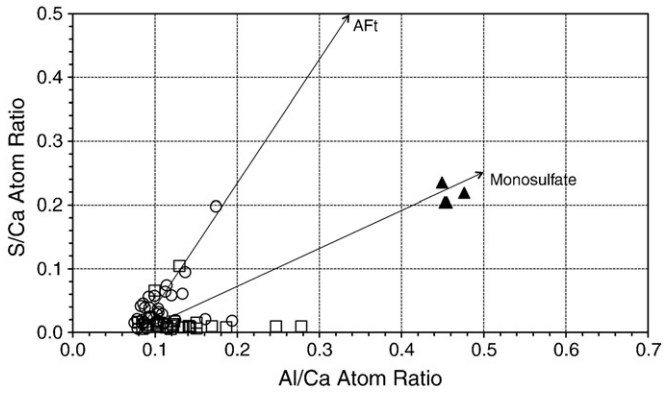

Fig. 18. S/Ca against Al/Ca atom ratio plot of TEM-EDX analyses of AFm (▲) and Op (○) and Ip (□) C–S–H present in the water-activated paste hydrated for 28 days.

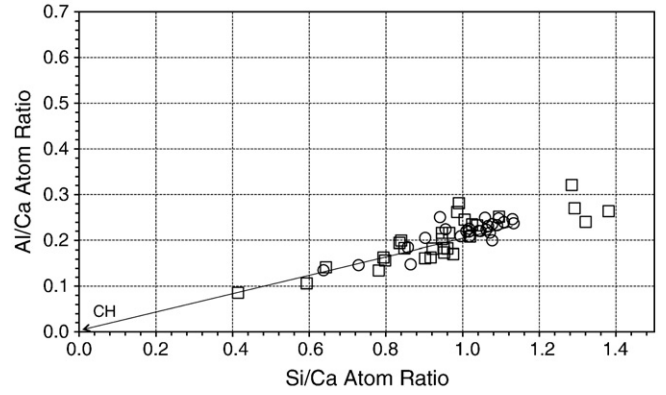

Fig. 19. Al/Ca against Si/Ca atom ratio plot of TEM-EDX analyses of Op (○) and Ip (□) C–S–H present in the KOH-activated paste hydrated for 28 days.

analysed crystals are essentially pure monosulfate, which is consistent with the XRD pattern.

Relicts of AFt crystals were not observed in the KOH-activated specimen, which is in agreement with the neat cement paste [12]. As a consequence, the Al/Ca against Si/Ca plot in Fig. 19 shows that none of the analyses contain a contribution from AFt. Whilst AFm phases can occur in KOH-activated cements [18], there is no contribution from such a phase in these data. The higher S/Ca values in Fig. 20 are clearly associated with enhanced K/Ca, Fig. 21; indeed the K/Ca and S/Ca values increase in an approximate 2:1 ratio, which suggests strongly that SO_4^{2-} ions are adsorbed on the C–S–H balanced by K^+ ions. The regression line indicates that the C–S–H itself has a K/Ca ratio of 0.17,

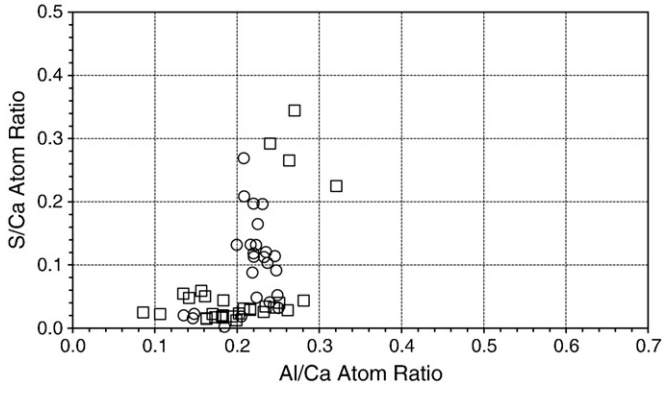

Fig. 20. S/Ca against Al/Ca atom ratio plot of TEM-EDX analyses of Op (○) and Ip (□) C–S–H present in the KOH-activated paste hydrated for 28 days.

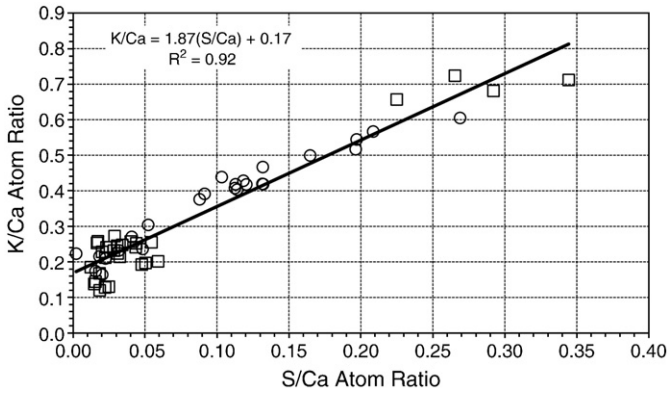

Fig. 21. K/Ca against S/Ca atom ratio plot of TEM-EDX analyses of Op (○) and Ip (□) C–S–H present in the KOH-activated paste hydrated for 28 days.

which is very similar to the Al/Ca ratio of the C–S–H (0.19), thus indicating that the potassium in the KOH-activated paste was present either within the C–S–H structure charge balancing the substitution of Al^{3+} for Si^{4+}, or adsorbed on the C–S–H charge balancing sulfate ions (i.e. a K/S ratio of 2). The four points for Ip on Fig. 19 that have particularly high Si/Ca ratios (and also high S/Ca and K/Ca, Fig. 21) were from the partially reacted fly ash particle shown in Fig. 15; the analyses probably correspond to a mixture of unreacted material from the fly ash and hydration product (with adsorbed K^+ and SO_4^{2-} ions).

Mean values of Ca/Si, Ca/(Al + Si) and Al/Si ratios for both Ip and Op C–S–H are given in Table 4. There is no statistically significant difference between the Al/Si ratios of the Ip and Op C–S–H with both water and KOH activation. The values measured in the TEM are lower than those determined by deconvolution of the NMR spectra when using only three C–S–H peaks (see discussion in Section 2). The mean Ca/(Al + Si) ratio of Ip C–S–H is lower than for Op C–S–H with water activation but higher with KOH; in both cases the difference is statistically significant. The mean value of the Ca/(Al + Si) ratio of the C–S–H present (both Ip and Op) in the KOH-activated paste (0.91) is significantly lower than with water activation (1.26). Comparison of the SEM-EDX data in Fig. 8 with the TEM-EDX data in Figs. 17 and 19 shows that the SEM analyses are in general richer in calcium; the difference between the mean values for the Ca/Si ratios determined by SEM-EDX and TEM-EDX (given in Tables 3 and 4 respectively) is statistically significant, so the SEM values are probably due to C–S–H intermixed with other phases, in particular microcrystals of CH.

3.5. Structural–chemical formulae for C–S–H

The TEM-EDX and NMR data in Tables 2 and 4 can be used to establish formulae for average structural units in the C–S–H in terms of the two alternative formulations for the nanostructure of C–S–H given by Richardson and Groves [19,21,22]; i.e. in terms of either the

Table 4
Mean Ca/Si, Ca/(Al + Si) and Al/Si atom ratios for both Op and Ip C–S–H in one-month-old samples obtained using TEM-EDX and Al/Si atom ratios determined by deconvolution of the single-pulse ^{29}Si MAS NMR spectra (S.D. = standard deviation; *N* = number of analyses).

			Ca/Si		Ca/(Al + Si)		Al/Si			
		N	Mean	S.D.	Mean	S.D.	Mean	S.D.	NMR no Q^{2B}	NMR with Q^{2B}
28 d water	Op	32	1.49	0.12	1.29	0.09	0.15	0.03		
	Ip	23	1.41	0.13	1.21	0.11	0.17	0.04		
	All	55	1.46	0.13	1.26	0.11	0.16	0.04	0.22	0.16
28 d KOH	Op	25	1.02	0.16	0.84	0.13	0.22	0.02		
	Ip	26	1.17	0.31	0.97	0.26	0.21	0.03		
	All	51	1.10	0.26	0.91	0.22	0.21	0.02	0.25	0.21

T/J or T/CH structural viewpoints. The T/J viewpoint envisages C–S–H to consist of structural elements based on the crystalline minerals 1.4 nm tobermorite (T) and jennite or jaffeite (J), whilst the T/CH viewpoint envisages elements of tobermorite-based structure interstratified with layers of CH-based structure. The models are discussed and illustrated in detail in [19]. The procedure to establish the structural formulae is straightforward: it simply involves calculation of the models' variables by inserting the experimentally determined mean values of Ca/Si and Al/Si ratios and aluminosilicate chain length into the formulae given in [14] and [18] (and summarized in [19]). So, for example, for the 28-day-old water-activated paste, an average structural unit with minimum degree of protonation of the aluminosilicate chains and assuming that the substitution of Si^{4+} by Al^{3+} is balanced entirely by Ca^{2+} ions, can be represented by Eq. (1):

$$\{Ca_{11.0}(Si_{0.86}Al_{0.14})_{15.6}O_{47.8}\}\cdot(OH)_{3.9}\cdot Ca_{8.6}\cdot mH_2O \quad (1)$$

The presence of hydroxyl groups outside the braces indicates that in terms of the T/J viewpoint, there must be some J-like structure. In terms of the T/CH viewpoint, the average structural unit is represented by Eq. (2):

$$Ca_{16.6}(Si_{0.86}Al_{0.14})_{15.6}O_{47.8}\cdot Ca_{1.1}\cdot 2Ca(OH)_2\cdot mH_2O \quad (2)$$

Repeating the same procedure for the KOH-activated paste — again assuming minimum degree of protonation of the aluminosilicate chains — but this time assuming that substitution of Si^{4+} by Al^{3+} is charge balanced entirely by K^+ ions, an average structural unit is represented by Eq. (3):

$$\{Ca_{7.6}H_{3.9}(Si_{0.83}Al_{0.17})_{10.4}O_{32.2}\}\cdot K_{1.8}\cdot Ca_{1.9}\cdot mH_2O \quad (3)$$

In this case, the minimum degree of protonation is quite high (about the level assumed in Taylor's model; see the discussion in reference [19]). The absence of hydroxyl groups outside the braces indicates that the structure is entirely T-based, with no J-like structure; the 1.9 calcium ions (i.e. $n-(w/2)$ ions) outside the braces are interlayer ions required for charge balance. In terms of the T/CH viewpoint, the average structural unit is represented by Eq. (4):

$$Ca_{9.5}H_{3.9}(Si_{0.83}Al_{0.17})_{10.4}O_{32.2}\cdot K_{1.8}\cdot mH_2O \quad (4)$$

It is evident that no CH-based layers are necessary.

In previous work it has for some systems been possible to suggest likely differences in the nanostructure of the C–S–H present in the inner and outer product microstructural regions [13,18] (when there are a reasonable number of TEM-EDX analyses of both Ip and Op C–S–H and the difference between their mean Ca/Si ratios is statistically significant). Following the same procedure outlined in those papers indicates that the aluminosilicate chains in the Op C–S–H were likely to be shorter than those present in the Ip C–S–H with water activation, but longer (and more protonated) with alkali.

4. Conclusions

The microstructure and composition of water- and alkali-activated hardened pastes of 70% white Portland cement–30% fly ash hydrated at 55 °C have been characterized using a multi-technique approach, with particular emphasis on the nature of the C–S–H phase. Comparison of the quantity of CH and the Al/Si ratio of C–S–H with the values for the neat cement pastes [12], indicates that some fly ash had reacted at 1 day, and a considerable amount by 28 days. The main crystalline hydration products were CH, AFt and AFm with water activation, and CH and a small amount of hydrogarnet with alkali; the CH formed in the alkali-activated system had a small average crystal size. Alkali activation resulted in C–S–H with slightly more structural order than with water. After 1-day hydration, the mean length of the aluminosilicate anions in the C–S–H was 4 with both methods of activation, and increased to 15.6 and 10.4 by 28 days with water and alkali respectively. Inner product C–S–H with a fine-scale, homogeneous morphology, was abundant in both systems and small, partially or fully reacted particles containing foil-like C–S–H were common. Outer product C–S–H was a mixture of fibrillar and foil-like morphology with water, and foil- or lath-like with alkali, both of which are consistent with previous observations at lower temperature. It was not possible to determine the chemical composition of C–S–H free of intermixture with other phases by X-ray analysis in the SEM; the higher resolution of TEM-EDX was necessary. The C–S–H formed in the alkali-activated paste had a lower mean Ca/(Al + Si) ratio than that formed with water. Inner product C–S–H had significantly lower Ca/Si and Ca/(Al + Si) ratios than outer product C–S–H with water activation, but both were higher with KOH. The aluminosilicate chains in the Op C–S–H were likely to be shorter than those present in the Ip C–S–H in the water-activated paste but longer (and more protonated) with alkali activation. The potassium in the KOH-activated paste was present either within the C–S–H structure charge balancing the substitution of Al^{3+} for Si^{4+}, or adsorbed on the C–S–H charge balancing sulfate ions (i.e. a K/S ratio of 2).

Acknowledgements

Thanks are due to the Engineering and Physical Sciences Research Council for funding under Grant No. GR/S45874/01, to Jason Boomer at W.R. Grace for conducting the XRD experiments and to Castle Cement, the Nuclear Decommissioning Authority, and Lafarge Cements for additional technical and financial support.

References

[1] H.F.W. Taylor, Cement Chemistry2nd edition, Thomas Telford Publishing, London, 1997.
[2] K.L. Scrivener, The effect of heat treatment on inner product C–S–H, Cem. Concr. Res. 22 (1992) 1224–1226.
[3] K.O. Kjellsen, R.J. Detwiler, O.E. Gjørv, Backscattered electron imaging of cement pastes hydrated at different temperatures, Cem. Concr. Res. 20 (1990) 308–311.
[4] Y. Cao, R.J. Detwiler, Backscattered electron imaging of cement pastes cured at elevated temperatures, Cem. Concr. Res. 25 (1995) 627–638.
[5] K.O. Kjellsen, Heat curing and post-heat curing regimes of high-performance concrete: influence in microstructure and C–S–H composition, Cem. Concr. Res. 26 (1996) 295–307.
[6] J.I. Escalante-Garcia, J.H. Sharp, Effect of temperature on the hydration of the main clinker phases in Portland cements: part I, neat cements, Cem. Concr. Res. 28 (1998) 1245–1257.
[7] J.I. Escalante-Garcia, J.H. Sharp, Variation in composition of C–S–H gel in Portland cement pastes cured at various temperatures, J. Am. Ceram. Soc. 82 (1999) 3237–3241.
[8] J.I. Escalante-Garcia, J.H. Sharp, The microstructure and mechanical properties of blended cements hydrated at various temperatures, Cem. Concr. Res. 31 (2001) 695–702.
[9] R. Yang, J.H. Sharp, Hydration characteristics of Portland cement after heat curing: I, degree of hydration of the anhydrous cement phases, J. Am. Ceram. Soc. 84 (2001) 608–614.
[10] R. Yang, J.H. Sharp, Hydration characteristics of Portland cement after heat curing: II, evolution of crystalline aluminate-bearing hydrates, J. Am. Ceram. Soc. 84 (2001) 1113–1119.
[11] C. Famy, K.L. Scrivener, A.K. Crumbie, What causes differences of C–S–H gel grey levels in backscattered electron images, Cem. Concr. Res. 32 (2002) 1465–1471.
[12] A.V. Girão, I.G. Richardson, C.B. Porteneuve, R.M.D. Brydson, Composition, morphology and nanostructure of C–S–H in white Portland cement pastes hydrated at 55 °C, Cem. Concr. Res. 37 (2007) 1571–1582.
[13] A.V. Girão, I.G. Richardson, R.M.D. Brydson, Composition, morphology and nanostructure of C–S–H in white Portland cement–fly ash blends hydrated at 85 °C, Adv. Appl. Ceram. 106 (2007) 283–293.
[14] I.G. Richardson, G.W. Groves, The structure of the calcium silicate hydrate phases present in hardened pastes of white Portland cement/blast-furnace slag blends, J. Mater. Sci. 32 (1997) 4793–4802.
[15] I.G. Richardson, The nature of C–S–H in hardened cements, Cem. Concr. Res. 29 (1999) 1131–1147.
[16] C.A. Love, I.G. Richardson, A.R. Brough, Composition and structure of C–S–H in white Portland cement–20% metakaolin pastes hydrated at 25 °C, Cem. Concr. Res. 37 (2007) 109–117.
[17] R. Taylor, I.G. Richardson, R.M.D. Brydson, Composition and microstructure of 20-year-old ordinary Portland cement-ground granulated blast-furnace slag blends containing 0 to 100% slag, Cem. Concr. Res. 40 (2010) 971–983.

[18] I.G. Richardson, A.R. Brough, G.W. Groves, C.M. Dobson, The characterization of hardened alkali-activated blast-furnace slag pastes and the nature of the calcium silicate hydrate (C–S–H) phase, Cem. Concr. Res. 24 (1994) 813–829.
[19] I.G. Richardson, Tobermorite/jennite and tobermorite/calcium hydroxide-based models for the structure of C–S–H: applicability to hardened pastes of tricalcium silicate, β-dicalcium silicate, Portland cement, and blends of Portland cement with blast-furnace slag, metakaolin or silica fume, Cem. Concr. Res. 34 (2004) 1733–1777.
[20] S.A. Rodger, G.W. Groves, Electron microscopy study of ordinary Portland cement and ordinary Portland cement-pulverized fuel ash blended pastes, J. Am. Ceram. Soc. 72 (1989) 1037–1039.
[21] I.G. Richardson, G.W. Groves, Models for the composition and structure of calcium silicate hydrate (C–S–H) gel in hardened tricalcium silicate pastes, Cem. Concr. Res. 22 (1992) 1001–1010.
[22] I.G. Richardson, G.W. Groves, The incorporation of minor and trace elements into calcium silicate hydrate (C–S–H) gel in hardened cement pastes, Cem. Concr. Res. 23 (1993) 131–138.